

The Capacity of Successive DF Relaying and Using Soft Multiple-Symbol Differential Sphere Detection

Li Li, Li Wang and Lajos Hanzo

School of ECS, University of Southampton, SO17 1BJ, United Kingdom.

Tel: +44-23-8059 3125, Fax: +44-23-8059 4508

Email: {ll5e08, lw5, lh}@ecs.soton.ac.uk, http://www-mobile.ecs.soton.ac.uk

Abstract—The conventional single-relay aided two-phase cooperative network employing a so-called soft-input soft-output multiple-symbol differential sphere detection (SISO-MSDSD) and operating in a distributed turbo decoding mode incurs a high complexity and imposes a 50% half-duplex relaying induced throughput loss. In this paper, we combat both of these critical problems. We commence by evaluating the Discrete-input Continuous-output Memoryless Channel (DCMC) capacity of the Decode-and-Forward (DF) based successive relaying aided networks (SRAN) as our theoretical benchmark. Then a relay-aided SISO-MSDSD is designed, which is then incorporated in the DF based SRAN. As our novel contribution, we demonstrate that the proposed transceiver is capable of significantly reducing the system's complexity, whilst recovering the 50% half-duplex relaying induced throughput loss. The system is capable of performing within 2.9 dB from the corresponding noncoherent DCMC capacity.

I. INTRODUCTION

As a benefit of their spatial diversity, Multiple-Input Multiple-Output (MIMO) techniques [1] are capable of efficiently mitigating the deleterious effects of Rayleigh fading channels. However, achieving transmit diversity in the uplink is impractical due to the limited antenna-separation of shirt-pocket-sized mobiles. Fortunately, the family of cooperation techniques heralded by van der Meulen in [2] is capable of achieving uplink transmit diversity by forming a virtual antenna array (VAA) in a distributed fashion. However, the conventional two-phase cooperative system incurs a severe multiplexing loss due to the half-duplex constraint of practical transceivers. A beneficial technique of recovering the multiplexing loss was advocated in [3], where the successive relaying regime was originally devised.

In order to eliminate the potentially complex channel estimation of coherent detection aided cooperative systems, which consumes extra energy and requires pilots that reduce the overall throughput, the family of low-complexity noncoherent detection arrangements dispensing with any channel estimation becomes an attractive design alternative. This is particularly so for a high number of antennas and for high Doppler frequencies, when the high-complexity coherent MIMOs suffer from high channel-estimation errors and might be outperformed by their low-complexity noncoherent counterparts [4].

Hence the Multiple-Symbol Differential Sphere Detection (MSDSD) algorithm was devised by Lampe *et al.* [5] for striking an attractive trade-off between the BER performance attained and the complexity imposed. Then, in order to transform the hard decision based MSDSD algorithm to a power-efficient, soft-decision-aided iterative detection scheme, the MSDSD algorithm was further developed to the soft-input soft-output MSDSD (SISO-MSDSD) regime in [6].

Against this background, our novel contributions are:

- 1) We derive the noncoherent Discrete-input Continuous-output Memoryless Channel (DCMC) capacity of the Decode-and-Forward (DF) based successive relaying aided networks (SRAN).

The financial support of the European Union under the auspices of the Newcom and Phoenix projects, as well as that of the RC-UK under the auspices of the India-UK Advanced Technology Centre known as IN-ATC is gratefully acknowledged.

- 2) Then, we specifically devise a relay-aided SISO-MSDSD algorithm, which is capable of combining the different received signal streams at the destination.
- 3) Finally, we demonstrate that by incorporating the relay-aided SISO-MSDSD decoder in the SRAN, the proposed transceiver significantly reduces the system complexity and recovers the half-duplex relaying induced throughput loss, while operating close to the corresponding system capacity.

The rest of this paper is organised as follows. Our system model is described in Section II. Section III derives the noncoherent DCMC capacity of the DF based SRAN. Then in Section IV, we design the proposed transceiver architecture. The robustness and throughput, as well as the system's complexity properties of the proposed transceiver are investigated by abundant simulations in Section V. Finally, we conclude in Section VI.

II. SYSTEM OVERVIEW

The typical network topology and transmission processes of the classic SRAN is portrayed in Fig.1, where the Mobile Station (MS) s , the activated relay stations (RS) r_1, r_2 and the Base Station (BS) d are specifically labelled. Additionally, the relays are assumed to be geographically isolated, and a frame-based transmission scheme associated with a fixed frame length of L is adopted.

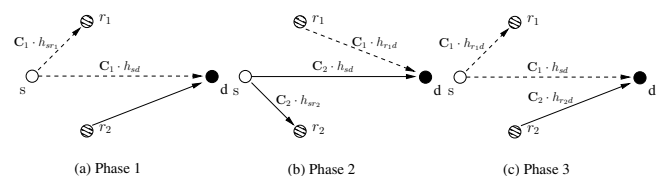


Fig. 1: Transmission processes of the SRAN, in different typical phases.

We use the notation $D_{i,j}, i, j \in \{s, r_1, r_2, d\}$ to represent the distance between node i and node j . Hence, the average path-loss gains of the Source-to-Relay link (SR_i) and Relay-to-Destination link (R_iD) with respect to the Source-to-Destination link (SD) are given by $G_{sr_i} = \left(\frac{D_{sd}}{D_{sr_i}}\right)^\alpha, i = 1, 2$ and $G_{r_i d} = \left(\frac{D_{sd}}{D_{r_i d}}\right)^\alpha, i = 1, 2$, respectively. Throughout this paper, the path-loss exponent is fixed to $\alpha = 3$ for representing a typical urban area. Then, to simplify our analysis, we assume that the SRAN has a symmetric topology, which implies that $D_{sr_1}, D_{r_1 d}, G_{sr_1}$ and $G_{r_1 d}$ are identical to $D_{sr_2}, D_{r_2 d}, G_{sr_2}$ and $G_{r_2 d}$, respectively. It is also assumed that we have $D_{sr_i} + D_{r_i d} \approx D_{sd}, i = 1, 2$ and D_{sd} is normalized to unity. Naturally, the above assumptions do not affect the general applicability of our analysis.

Furthermore, all the possible propagation paths between the s, r_i and d are assumed to be time-selective block-fading Rayleigh channels [7], where the fading coefficients $h_{i,j}[k], i, j \in \{s, r_1, r_2, d\}$ fluctuate according to the normalized Doppler frequency in a block and change according to an independent and identical distribution (i.i.d) from one block to the next [8]. The correlated fading block length of such channel is represented by T_b .

As detailed in [9], one of the most important features of SRAN is that the signals $c_s[k]$ transmitted by the source node (SN) and the signals $c_{r_i}[k], i = 1, 2$ forwarded by the relay node

(RN) can always be assumed to be simultaneously received at the destination. However, $c_s[k]$ and $c_{r_i}[k]$ correspond to different original information symbols. Hence they potentially interfere with each other. Fortunately, the reduction of the successive relaying induced interference between the transmitted signals of the source and the relay has been solved in [10] with the aid of DS-CDMA and a specifically designed spread-despread regime, where the exact components and detailed formulas of the despread signals were also provided.

Hence, with the aid of the spreading regime in [10], as well as employing two orthogonal binary DS spreading codes, namely $\mathbf{C}_i, i = 1, 2$ having a spreading factor of Q , the n^{th} received signal of the l^{th} frame at the destination may be formulated as ¹

$$y_i[k] = \sqrt{G_{sd}}h_{sd}[k]c_s[k] + \sqrt{G_{r_i d}}h_{r_i d}[k]c_{r_i}[k] + n_d[k], \quad (1)$$

where $i = 1, 2$ and $k = l \cdot L + n$.

When employing the DF protocol, we have $c_s[k] = s[k] \cdot \mathbf{C}_i$ and $c_{r_i}[k] = r_i[k] \cdot \mathbf{C}_{\bar{i}}$, where $s[k]$ and $r_i[k]$ represent the modulated symbol at the SN s and the remodulated symbol at the RN r_i , respectively. The operation \bar{i} is defined as ($\bar{1} = 2$) and ($\bar{2} = 1$). If the RN correctly decodes the received source signals and re-encodes as well as remodulates them using the same schemes as that of the SN, then we attain $c_{r_i}[k] = s[k - L] \cdot \mathbf{C}_{\bar{i}}$. We note that $c_{r_i}[k]$ corresponds to the $(k - L)^{\text{th}}$ modulated source symbol $s[k - L]$, instead of corresponding to the k^{th} modulated source symbol $s[k]$, which happens to be the n^{th} modulated source symbol of the current frame. This particular property of the SRAN is also mentioned in [9, (Fig.1d)].

Then, the different components of the received signal $y_i[k]$ can be resolved by appropriately configuring the chip-waveform matched-filter for the different spreading codes, as depicted by the despread regime in [10]. Hence, when the DF protocol is employed, the despread signal extracted from $y_i[k]$ and dominated by the SN's transmitted signal $c_s[k]$ can be represented as

$$z_i^s[k] = M_s[k] + I_{r_i}[k] + n_d[k] \quad (2)$$

where the main component $M_s[k]$ of the despread signal and the interference component $I_{r_i}[k]$ are formulated as

$$M_s[k] = \sqrt{G_{sd}}h_{sd}[k]s[k] \quad (3)$$

$$I_{r_i}[k] = \frac{1}{Q} \sqrt{G_{r_i d}}h_{r_i d}[k]r_i[k]. \quad (4)$$

Symmetrically, the despread signal extracted from $y_i[k]$ but dominated by the RN's forwarded signal $c_{r_i}[k]$ can be represented as

$$z_i^{r_i}[k] = M_{r_i}[k] + I_s[k] + n_d[k], \quad (5)$$

where $M_{r_i}[k]$ and $I_s[k]$ are given by $Q \cdot I_{r_i}[k]$ and $\frac{1}{Q} \cdot M_s[k]$, respectively.

III. NONCOHERENT DCMC CAPACITY OF DF BASED SRAN

As mentioned above, noncoherent detection will be employed. Hence we focus our attention on deriving the noncoherent DCMC capacity of the DF based SRAN, and in Section V we will exploit it as an important benchmark.

The transmission arrangement of the twin-relay-aided successive relaying procedure can be viewed as the superimposed transmissions of two conventional single-relay aided two-phase cooperative networks [9]. This is also illustrated in Figure 1, where the transmissions represented by dashed lines in phase 1 and 2

¹Actually, the received signal $y_i[k]$, the transmitted signal $c_s[k]$, $c_{r_i}[k]$ and the AWGN noise $n_d[k]$ are Q -element vectors due to the spreading operation. Nevertheless, we still represent them in a variable form to simplify the representations of the relevant equations, which does not affect the validity of the results.

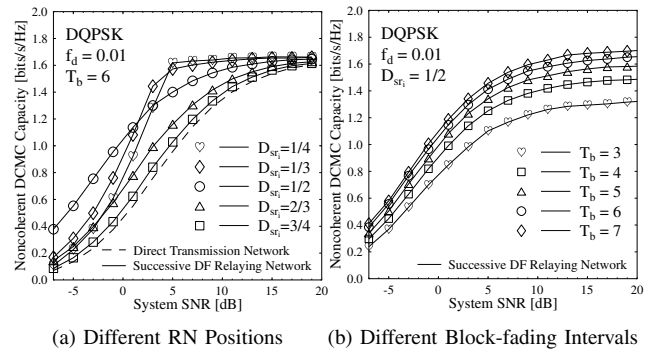


Fig. 2: The noncoherent DCMC capacity of the DF based SRAN, where normalized Doppler frequency of $f_d = 0.01$ and DQPSK modulation are assumed.

constitute one of the conventional single-relay aided two-phase cooperative networks, namely Coop-I. Similarly, the transmissions represented by the solid lines in phase 2 and 3 constitute another one, namely Coop-II. Correspondingly, the noncoherent DCMC capacity of the DF based SRAN is also constituted by the sum of the capacities of the DF based sub-network Coop-I and Coop-II, which is formulated as follows

$$C_{Successive}^{DF} = C_{Coop-I}^{DF} + C_{Coop-II}^{DF}, \quad (6)$$

providing that the successive relaying induced interference has been sufficiently mitigated by the DS-CDMA technique and using a large spreading factor Q .

Fortunately, the noncoherent DCMC capacity of the DF based conventional single-relay aided two-phase cooperative network has been evaluated in [11]. Additionally, in order to achieve perfectly correct detection at the RN and thus to avoid any potential error propagation, the source transmission rate should be lower than the noncoherent information rate of the SR link. Based on this constraint, C_{Coop-I}^{DF} may be evaluated by

$$C_{Coop-I}^{DF} = \min\{\beta I_{s,r_i}, \beta I_{s,d} + (1 - \beta)I_{r_i,s}\}, \quad (7)$$

where the time resource allocation (TRA) factor of $\beta = \frac{T_s}{T_s + T_r}$. T_s and T_r represent the broadcast phase and cooperation phase duration, respectively. Then $I_{i,j}$ represents the noncoherent information rate of the single link from node i to node j .

For the sake of simplifying the analysis, we equally split the time between the broadcast and cooperation phases. Furthermore, we assume that the overall transmit power P is equally allocated, which means the average transmit power of the i^{th} RN and of the SN have the relation that $P_{r_i} = P_s = \frac{1}{2}P$.

A simple cooperative-user-selection scheme was employed, where only the effect of the geometrical position of the RN was considered. The simulation based capacity results $C_{Successive}^{DF}$ associated with different SR distances of $D_{sr_i} \in \{\frac{1}{4}, \frac{1}{3}, \frac{1}{2}, \frac{2}{3}, \frac{3}{4}\}$ are displayed in Fig.2a, where the block-fading length is fixed to $T_b = 6$. Observe in Fig.2a that our DF based SRAN is better to appoint RNs, which roam closer to the SN, rather than to the DN for the sake of achieving a higher capacity. In this paper, we configured our system to operate at low SNRs, since the transmit power has to be minimized in most practical applications. Naturally, this limits the attainable throughput. Accordingly, observe in Fig.2a that, in the SNR region below 1.5 dB, the DF based system appointing a RN at the position of $D_{sr_i} = \frac{1}{2}$ achieves the highest capacity. In order to characterize the capacity of the DF based SRAN further, the effect of the block-fading intervals is portrayed in Fig.2b, where different T_b values associated with different detection complexities are considered.

IV. RELAY-AIDED SISO-MSDSD ASSISTED ITERATIVE DECODING FOR SUCCESSIVE RELAYING

The transceiver architecture specifically designed for our DF based SRAN is portrayed in Fig.3. At the SN, we use a conventional differentially encoded modulator, such as DQPSK, which is further combined with a unity-rate-code (URC) encoder. Furthermore, a conventional half-rate RSC is employed as the outer code. Hence a three-stage RSC-URC-DM source encoder is created. The corresponding receiver proposed for the relay consists of

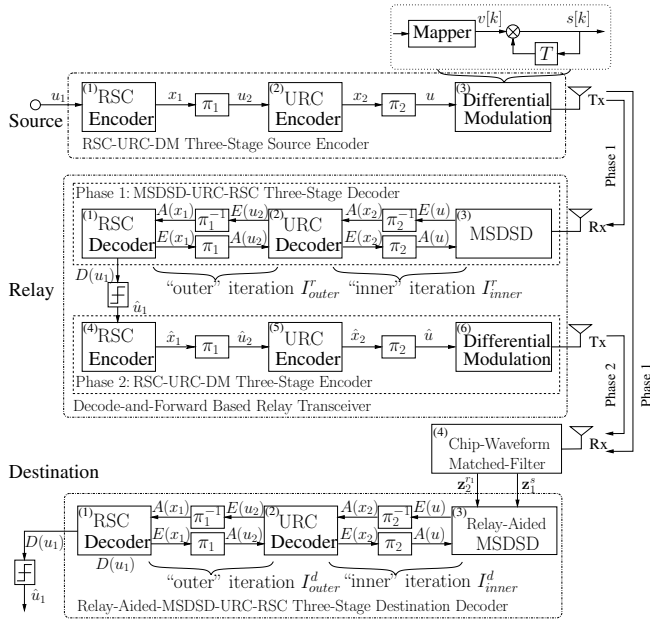


Fig. 3: Schematic of the proposed transceiver in our DF based SRAN.

three stages, namely the conventional single-path SISO-MSDSD [6] based soft decoder, the URC decoder and the RSC decoder. The *extrinsic* information and *a priori* information, represented by $E(\cdot)$ and $A(\cdot)$ respectively, are interleaved and iteratively exchanged within the two-stage inner decoder I_{inner}^r times, before the result is further exchanged between the inner and outer decoders I_{outer}^r times. The motivation of employing this three-stage concatenated decoder architecture is to improve the convergence behavior of the iterative decoder with the aid of the URC decoder, as detailed in [4]. The URC model has an infinite impulse response (IIR) due to its recursive encoder structure, consequently the EXIT curve of the URC aided inner decoder is capable of approaching the point of perfect convergence at (1.0, 1.0) in the EXIT chart. Hence, no error floor is expected. Therefore, the receiver of the RN is capable of near-perfectly detecting the signals received from the SN during phase 1, consequently generating the correct estimates of the original source bits, namely \hat{u}_1 , at as low SNR values as possible. As a benefit, the error propagation problem of the DF scheme is avoided. The RN's transmitter is designed to be identical to the three-stage RSC-URC-DM encoder of the SN. Hence, if the estimates \hat{u}_1 are correctly generated by the RN's receiver in phase 1, the differentially modulated symbols produced by the RN's transmitter during phase 2 will be the same as $s[k]$. Furthermore, the proposed SISO-MSDSD decoder is also employed at the DN, where we have to ensure that its multiple input signal streams are appropriately time-aligned, so that they correspond to the same differentially modulated symbols.

Before introducing the DN's receiver design, we first analyse the proposed SISO-MSDSD algorithm. Initially, the SISO-MSDSD algorithm advocated by Pauli *et al.* in [6] was invoked for iterative decoding in the direct transmission system. We further developed

it to ensure that it becomes capable of simultaneously dealing with multiple input signal streams, where the multiple input signal streams are associated with the same modulated symbols. Hence the resultant modified SISO-MSDSD algorithm is invoked for iterative decoding in the context of our cooperative network, which is consequently termed as the relay-aided SISO-MSDSD. Instead of processing a single received signal stream, our relay-aided SISO-MSDSD evaluates the *a posteriori* LLR of the μ^{th} bit $u[\mu]$ by simultaneously processing Ω received signal streams represented by $\{\mathbf{z}_\lambda\}_{\lambda=1,2,\dots,\Omega}$ as follows

$$L_u[\mu] = \ln \frac{\Pr(u[\mu] = b | \{\mathbf{z}_\lambda\}_{\lambda=1,2,\dots,\Omega})}{\Pr(u[\mu] = \bar{b} | \{\mathbf{z}_\lambda\}_{\lambda=1,2,\dots,\Omega})}, \quad b \in \{0, 1\}, \quad (8)$$

where \bar{b} is the complement of b . The resultant relay-aided SISO-MSDSD decoder is employed as the first stage of the overall iterative receiver at the DN, which is then further amalgamated with the URC decoder in order to form a two-stage inner decoder for appropriately complementing the SN's and RN's transmitter architecture. The SN's transmitted signal $s[k]$ is received at the destination during Phase 1, which is then despread, as described in Section II, yielding the despread signal $z_1^s[k]$ of (2). Another replica of $s[k]$ is forwarded by the RN, which arrives at the DN after a one-frame delay and generates the despread signal $z_2^{r1}[k+L]$ formulated in (5) during Phase 2. Finally, upon substituting the streams of $\mathbf{z}_1^s = [z_1^s[k+1], z_1^s[k+2], \dots, z_1^s[k+T_b]]^T$ and $\mathbf{z}_2^{r1} = [z_2^{r1}[k+1+L], z_2^{r1}[k+2+L], \dots, z_2^{r1}[k+T_b+L]]^T$ into (8) as $\{\mathbf{z}_\lambda\}_{\lambda=1,2}$, (8) can be rewritten with the aid of Bayes' theorem as

$$\begin{aligned} L_u[\mu] &= \ln \frac{\Pr(u[\mu] = b | \mathbf{z}_1^s, \mathbf{z}_2^{r1})}{\Pr(u[\mu] = \bar{b} | \mathbf{z}_1^s, \mathbf{z}_2^{r1})} \\ &= \ln \frac{\sum_{\mathbf{v} \in \mathcal{X}_{:u[\mu]=b}} \Pr(\mathbf{z}_1^s | \mathbf{v}) \Pr(\mathbf{z}_2^{r1} | \mathbf{v}) \Pr(\mathbf{v})}{\sum_{\mathbf{v} \in \mathcal{X}_{:u[\mu]=\bar{b}}} \Pr(\mathbf{z}_1^s | \mathbf{v}) \Pr(\mathbf{z}_2^{r1} | \mathbf{v}) \Pr(\mathbf{v})}, \quad (9) \end{aligned}$$

where the $(T_b - 1)$ -element vector \mathbf{v} consists of the QPSK symbols generated after the required bit-to-symbol mapping. The relationship of the symbol-vector \mathbf{v} and \mathbf{s} becomes explicit in the model seen at the top-right corner of Fig.3, where we have $\mathbf{s} = [s[k+1], s[k+2], \dots, s[k+T_b]]^T$. Furthermore, $\mathcal{X}_{:u[\mu]=b}$ represents the set of $\frac{M_c^{T_b-1}}{2}$ number of legitimate transmitted vectors \mathbf{v} , whose μ^{th} bit is constrained to $u[\mu] = b$, and similarly, $\mathcal{X}_{:u[\mu]=\bar{b}}$ is defined as the set corresponding to $u[\mu] = \bar{b}$. Based on (9) and invoking the "sum-max" approximation, the *a posteriori* LLR of $u[\mu]$ may be further approximated by

$$\begin{aligned} L_u[\mu] &\approx \ln \frac{\max_{\mathbf{v} \in \mathcal{X}_{:u[\mu]=b}} \exp\{-\|\mathbf{U}^s \mathbf{s}\|^2 - \|\mathbf{U}^{r1} \mathbf{s}\|^2 + \ln \Pr(\mathbf{v})\}}{\max_{\mathbf{v} \in \mathcal{X}_{:u[\mu]=\bar{b}}} \exp\{-\|\mathbf{U}^s \mathbf{s}\|^2 - \|\mathbf{U}^{r1} \mathbf{s}\|^2 + \ln \Pr(\mathbf{v})\}} \\ &= -\|\mathbf{U}^s \hat{\mathbf{s}}_{\text{MAP}}^b\|^2 - \|\mathbf{U}^{r1} \hat{\mathbf{s}}_{\text{MAP}}^b\|^2 + \ln \Pr(\hat{\mathbf{v}}_{\text{MAP}}^b) \\ &\quad + \|\mathbf{U}^s \hat{\mathbf{s}}_{\text{MAP}}^{\bar{b}}\|^2 + \|\mathbf{U}^{r1} \hat{\mathbf{s}}_{\text{MAP}}^{\bar{b}}\|^2 - \ln \Pr(\hat{\mathbf{v}}_{\text{MAP}}^{\bar{b}}), \quad (10) \end{aligned}$$

where \mathbf{U}^s can be attained by $\mathbf{U}^s \triangleq (\mathbf{F} \text{diag}\{\mathbf{z}_1^s\})^*$, with \mathbf{F} being an upper-triangular matrix obtained by the Cholesky factorization of the matrix $(P_s \mathcal{E}\{\mathbf{h}_{sd} \mathbf{h}_{sd}^H\} + 2\sigma_w^2 \mathbf{I}_{T_b})^{-1}$, when ignoring the successive relaying induced interference, which is kept low by using a sufficiently high spreading factor of Q . Explicitly, \mathbf{U}^{r1} can be calculated by a similar method, where \mathbf{F} is given this time by the Cholesky factorization of the matrix $(G_{r1d} P_{r1} \mathcal{E}\{\mathbf{h}_{r1d} \mathbf{h}_{r1d}^H\} + 2\sigma_w^2 \mathbf{I}_{T_b})^{-1}$. Still referring to (10), $\hat{\mathbf{s}}_{\text{MAP}}^b$ is one of the legitimate differentially encoded DQPSK symbol vectors \mathbf{s} , which maximizes the term $\{-\|\mathbf{U}^s \mathbf{s}\|^2 - \|\mathbf{U}^{r1} \mathbf{s}\|^2 + \ln \Pr(\mathbf{v})\}$ involved in the numerator of (10). The signal vector $\hat{\mathbf{s}}_{\text{MAP}}^b$ can be attained by implementing a specific sphere detection (SD) algorithm, which is similar to that described in [10], and additionally constraining the SD's search space to $\mathcal{X}_{:u[\mu]=b}$. Then $\hat{\mathbf{v}}_{\text{MAP}}^b$ is the corresponding

QPSK symbol vector, which is uniquely identified by $\hat{\mathbf{s}}_{\text{MAP}}^b$. Similarly, if the SD's search space is fixed to $\mathcal{X}:u[\mu]=\bar{b}$, $\hat{\mathbf{s}}_{\text{MAP}}^b$ and $\hat{\mathbf{v}}_{\text{MAP}}^b$ are readily obtained.

Our complexity comparison between the single-path SISO-MSDSD decoder advocated in [6] and the proposed relay-aided SISO-MSDSD decoder is provided in Fig.4. In the spirit of [6], the average number of real-valued multiplication operations (RMO) required for generating a soft-output during the SISO-MSDSD detection once per iteration is employed here as our complexity measure. If the time-selective block-fading channel associated with a correlated fading block length of $T_b = 6$, and a normalized Doppler frequency of $f_d = 0.01$ are assumed, the SNR values of 6.05 dB and 0.82 dB represent the corresponding ‘‘turbo-cliff’’ points in Fig.5b for the single-path SISO-MSDSD assisted system and for the relay-aided SISO-MSDSD assisted system, respectively. We will return to these issues later in the context of Fig.5b. For the sake of a fair comparison, we ensured that both the conventional single-path SISO-MSDSD decoder and the relay-aided SISO-MSDSD decoder operated near their associated ‘‘turbo-cliff’’ points. Then we varied the *a priori* mutual information of the two different SISO-MSDSD decoders and recorded the associated number of RMO required for producing a single soft-output in once iteration. It is demonstrated in Fig.4 that the proposed relay-aided SISO-MSDSD decoder approximately doubles the complexity compared to the single-path SISO-MSDSD decoder right across the entire *a priori* mutual information region considered. The

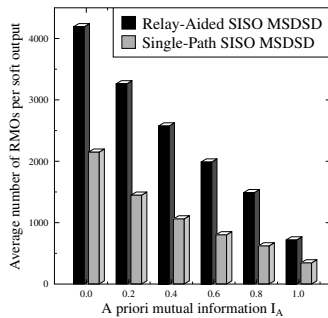


Fig. 4: Complexity of two different SISO-MSDSD decoders at different *a priori* mutual information values.

remaining components of the DN's receiver are similar to the those of the RN, hence they affect the overall complexity in a similar way.

When designing an iterative decoding aided cooperative system, the distributed turbo coding scheme advocated in [12] is attractive, since it is capable of simultaneously benefiting from both the interleaving-induced increased time-diversity gain at the RN, as well as from the iterative decoding gain at the DN attained by the iterative information exchange between the direct and relayed versions of the same codeword. Naturally, the improved system performance is achieved at the cost of increasing the complexity imposed by employing an extra decoder stage.

Naturally, the proposed relay-aided SISO-MSDSD algorithm constitutes a realistic method of maintaining a low complexity, where the combination of the information provided by the direct and relayed signal streams, namely by \mathbf{z}_1^i and \mathbf{z}_2^i is achieved without an extra iteration stage. More explicitly, in a cooperative network, where the distributed turbo coding principle is employed by invoking the single-path SISO-MSDSD algorithm, as in [8], each input signal stream is first individually processed by a single-path SISO-MSDSD aided turbo decoder within the inner iterative stage of [8, (Fig.5)]. Then the resultant information is passed on to the outer iterative stage of [8, (Fig.5)], and typically at least two iterations are carried out in order to exchange information between

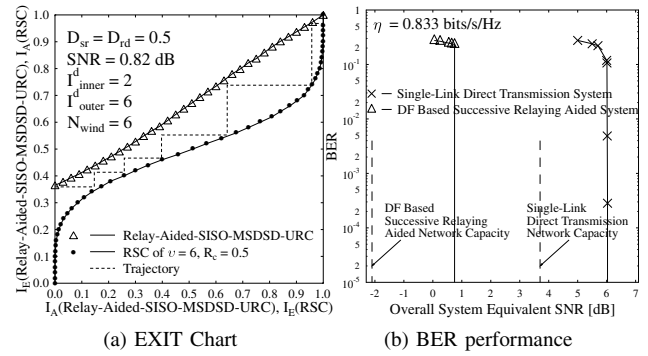


Fig. 5: The EXIT characteristic of our proposed destination receiver and the BER performances corresponding to different systems.

the different input signal streams. Hence, based on our complexity comparison in Fig.4, it is reasonable to argue that our three-stage relay-aided-MSDSD-URC-RSC decoder is capable of halving the system complexity imposed by the conventional single-path SISO-MSDSD aided distributed turbo decoder.

V. SIMULATION RESULTS AND ANALYSIS

Based on the analysis provided in Sections III and IV, all the system parameters adopted in our forthcoming simulations obey Table I, except when we provide different specific interpretations. We use an interleaver frame length of 480×10^3 symbols in order to eliminate the fading-induced correlations among the symbols of different decision blocks for the sake of achieving efficient iterative decoding.

Channel Model	Time-Selective Block-Fading Channel
Path-Loss Exponent	$\alpha = 3$
Correlated Fading Block Length	$T_b = 6$
Normalized Doppler Frequency	$f_d = 0.01$
Channel Coding	RSC Code
Code Memory Length	$\nu = 6$
Code Rate	$R_c = 0.5$
Modulation	DQPSK
MSDSD Observation Window Size	$N_{wind} = 6$
Inner Iterations of DN's Decoder	$I_{inner}^d = 2$
Outer Iterations of DN's Decoder	$I_{outer}^d = 6$
Relay Position	$D_{sr_i} = \frac{1}{2}; G_{sr_i} = G_{r_i d} = 8$
Overall Bandwidth efficiency	$\eta = 0.8333$ bits/s/Hz

TABLE I: SYSTEM PARAMETERS

A. BER versus SNR

Let us now investigate the robustness of the proposed three-stage relay-aided-MSDSD-URC-RSC scheme in terms of its BER performance. We commence by identifying the ‘‘turbo-cliff’’ SNR with the aid of Extrinsic Information Transfer (EXIT) Charts, as detailed in [13]. The relevant EXIT-chart and BER results of the proposed transceiver are shown in Fig.5.

Observe in Fig.5a that an open tunnel exists between the EXIT curves of the two-stage relay-aided-MSDSD-URC inner decoder and the outer RSC decoder, when the overall equivalent SNR value² reaches 0.82 dB where the associated Monte-Carlo simulation based decoding trajectory relying on a frame length of $L = 960 \times 10^3$ bits is also provided. This trajectory closely matches the EXIT curves and demonstrates that $I_{outer}^d = 6$ outer iterations are sufficient for our system to approach the point of perfect convergence at (1.0, 1.0) in the EXIT chart. Consequently, an infinitesimally low BER is expected beyond the point of SNR = 0.82 dB.

²Here the terminology of ‘equivalent SNR’ is defined as the ratio of the transmit power with respect to the receiver's noise, which is unconventional in the sense that it is measured at physically different points. However, this definition is convenient for the relay-aided system considered.

This is further evidenced in Fig.5b, where the capacity of the proposed DF based SRAN is also characterized, as inferred from Fig.2. In our case, the corresponding bandwidth efficiency is $\eta \approx R_c \times \log_2 M_c \times \frac{T_b-1}{T_b} = 0.8333$ bit/s/Hz. The proposed transceiver architecture of Fig.3 exhibits a performance within 2.9 dB from the capacity of the DF based SRAN. This 2.9 dB discrepancy may be further reduced for example with the aid of an irregular outer code, as detailed for example in [4]. To elaborate a little further, observe in Fig.5b that an approximately 5.2 dB power reduction is achieved by the proposed DF scheme in comparison to the classic direct transmission regime.

B. Throughput versus Complexity

The conventional time-selective Rayleigh fading channel having a normalized Doppler frequency of $f_d = 0.01$ is assumed in this subsection. Then, according to the properties of EXIT charts [13], the area under the soft-demodulator's bit-based EXIT curve, namely \mathcal{A} , determines the maximum achievable coding rate of the outer channel encoder, while guaranteeing near-error-free transmission for a normalized throughput below this value. Hence the maximum achievable throughput of the proposed DF based SRAN experiencing a conventional time-selective Rayleigh fading channel is given by

$$\mathcal{T}_{max} = \log_2 M_c \cdot \mathcal{A} \quad \text{bits/s/Hz.} \quad (11)$$

It is demonstrated in Fig.6a that the maximum achievable throughput can be improved by increasing the observation window size of the relay-aided SISO-MSDSD decoder. However, this throughput improvement is achieved at the cost of imposing an increased complexity on the system, especially on the relay-aided SISO-MSDSD decoder. Hence we further compare the system's complexity imposed by employing different observation window sizes N_{wind} . Naturally, the total complexity can be evaluated as

$$\mathcal{C}_{total} \triangleq \mathcal{I}_{iter} \times \mathbf{E}(\mathcal{C}_{per-iter}), \quad (12)$$

for different inner codes, where \mathcal{I}_{iter} represents the number of iterations within the open tunnel between the inner and outer decoder's EXIT curve required for approaching the point of perfect convergence at (1.0, 1.0) in the EXIT chart, while $\mathbf{E}(\mathcal{C}_{per-iter})$ is the average system complexity imposed during a single iteration.

As described in [13], the EXIT curve of the optimum outer code, which is capable of attaining the maximum achievable throughput should perfectly match the EXIT curve of the inner codes, namely that of the demodulator. Consequently, an extremely narrow open tunnel will occur between the outer and inner code's EXIT curve. As a penalty, a high \mathcal{I}_{iter} value is required. Hence we may readily assume that optimum outer codes matched to different inner codes having different observation window sizes require a similar value of \mathcal{I}_{iter} . Consequently, instead of comparing \mathcal{C}_{total} , we may directly use $\mathbf{E}(\mathcal{C}_{per-iter})$ for our complexity comparisons, where the proportionality of the complexity associated with different observation window sizes remains. Such optimum outer codes may be designed, for example using irregular convolutional codes, where only the coding rates of the individual constituent sub-codes are different. Hence only the complexity imposed by the relay-aided SISO-MSDSD decoder has to be involved in the complexity comparison.

Based on the above analysis, we first fix the observation window size. Then we gradually increase the *a priori* mutual information of the relay-aided SISO-MSDSD decoder from 0.0 to 1.0 by a step-size of 0.02 and employ the average of all the recorded RMO per bit values associated with each of the iterations as an approximation of $\mathbf{E}(\mathcal{C}_{per-iter})$. After implementing this approximation process for each N_{wind} value considered, the trade-off between

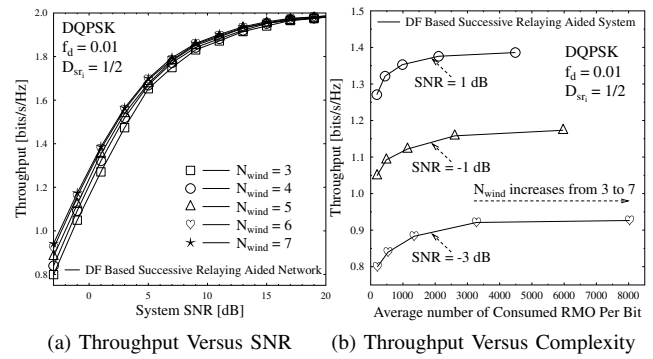


Fig. 6: The trade-off between the maximum achievable throughput and the complexity per bit, where various values of N_{wind} are investigated.

the maximum achievable throughput and the complexity imposed is visualized in Fig.6b, where different SNR values are considered.

VI. CONCLUSIONS

In this contribution, based on the capacity analysis of Section III and the simulation results of Section IV, we may reasonably conclude that instead of invoking the distributed turbo coding regime of [12], which inherently leads to the employment of the conventional single-path SISO-MSDSD decoder, our proposed transceiver was specifically designed for the DF based SRAN, which allowed us to halve the system complexity. Furthermore, a power reduction of about 5.2 dB was attained with respect to its direct transmission based counterparts.

REFERENCES

- [1] G. J. Foschini and M. J. Gans, "On Limits of Wireless Communications in a Fading Environment when Using Multiple Antennas," *Wireless Personal Communications*, vol. 6, pp. 311–335, Mar 1998.
- [2] Van der Meulen, E.C., "Three-Terminal Communication Channels," *Advanced Applied Probability*, vol. 3, pp. 120–154, 1971.
- [3] Y. Fan, C. Wang, J. Thompson, H. V. Poor, "Recovering Multiplexing Loss through Successive Relaying Using Repetition Coding," *IEEE Transactions on Communications*, vol. 6, pp. 4484–4493, December 2007.
- [4] L. Hanzo, Y. Akhtman, M. Jiang and L. Wang, "MIMO-OFDM for LTE, WIFI and WIMAX: Coherent versus Non-Coherent and Cooperative Turbo-Transceivers," *John Wiley*, 2010.
- [5] L. Lampe, R. Schober, V. Pauli, and C. Windpassinger, "Multiple-Symbol Differential Sphere Decoding," *IEEE Transactions on Communications*, vol. 12, pp. 1981–1985, Dec 2005.
- [6] V. Pauli, L. Lampe, and R. Schober, "Turbo DPSK" Using Soft Multiple-Symbol Differential Sphere Decoding," *IEEE Transactions on Information Theory*, vol. 52, pp. 1385–1398, April 2006.
- [7] Y. B. Liang and V. V. Veeravalli, "Capacity of Noncoherent Time-Selective Block Rayleigh Flat-Fading Channel," *IEEE International Symposium on Information Theory*, p. 166, 2002.
- [8] L. Wang, L. K. Kong, S. X. Ng and L. Hanzo, "A Near-Capacity Differentially Encoded Non-Coherent Adaptive Multiple-Symbol-Detection Aided Three-Stage Coded Scheme," *Vehicular Technology Conference*, vol. 1, pp. 1–5, May 2010.
- [9] L. K. Kong, S. X. Ng, R. G. Maunder, and L. Hanzo, "Near-Capacity Cooperative Space-Time Coding Employing Irregular Design and Successive Relaying," *IEEE Transactions on Communications*, vol. 58, pp. 2232–2241, August 2010.
- [10] L. Li and L. Hanzo, "Multiple-Symbol Differential Sphere Detection Aided Successive Relaying in the Cooperative DS-CDMA Uplink," *WCNC* <http://eprints.ecs.soton.ac.uk/21931/>, March 2011.
- [11] L. Wang, L. Kong, S. X. Ng and L. Hanzo, "To Cooperate or Not: A Capacity Perspective," *Vehicular Technology Conference*, May 2010.
- [12] B. Zhao and M. C. Valenti, "Distributed Turbo Coded Diversity for Relay Channel," *Electronics Letters*, vol. 39, pp. 786–787, May 2003.
- [13] A. Ashikhmin, G. Kramer and S. ten Brink, "Extrinsic information transfer functions: model and erasure channel properties," *IEEE Transactions on Information Theory*, vol. 50, pp. 2657–2673, Nov 2004.